



# Arecibo Investigations of Pulsar B0823+26. I. Plasma Source Changes Configure Its Bright and Quiet Modes

Joanna M. Rankin<sup>1,2</sup> , Timothy E. E. Olszanski<sup>1,3</sup>, and Geoffrey A. E. Wright<sup>4</sup>

<sup>1</sup> Physics Department, University of Vermont, Burlington, VT 05405, USA; [Joanna.Rankin@uvm.edu](mailto:Joanna.Rankin@uvm.edu)

<sup>2</sup> Anton Pannekoek Institute for Astronomy, University of Amsterdam, Science Park 904, 1098 XH Amsterdam, The Netherlands

<sup>3</sup> Physics and Astronomy Department, P.O. Box 6315, West Virginia University, Morgantown, WV 26506, USA

<sup>4</sup> Jodrell Bank Centre for Astrophysics, University of Manchester, Manchester M13 9PL, UK

Received 2019 September 2; revised 2019 December 30; accepted 2019 December 30; published 2020 February 24

## Abstract

The recently discovered 100X weaker quiescent (Q) mode in pulsar B0823+26 is X-ray quiet, unlike its usual bright (B) mode. Arecibo polarimetric observations were conducted to confirm the pulsar’s orthogonal geometry and investigate the emission associated with its main pulse (MP), interpulse (IP), and postcursor (PC) components. Main results: (1) the pulsar’s MP, PC, and IP are present in both modes and exhibit a two-pole orthogonal geometry. (2) The B-mode MP is dominated by core emission with weak conal outriders, whereas, the Q-mode double profile shows mainly residual conal emission with little core. The IP is conal in both modes. (3) Sporadic intrapulse emission trailing the PC is detected in the Q mode. (4) B0823+26 falls close to an  $\dot{E}$  boundary of  $10^{32.5}$  erg s<sup>-1</sup> (or  $B_{12}/P^2 \sim 2.5$ ) between core- and conal-dominated profiles—which also represents a boundary between pair-plasma source configurations above the polar cap. For larger energies, the pair-formation front is central, flat, and generates backflow heating, whereas for smaller energies it is peripheral, lower, and produces little heating. (5) Apparently, the pulsar is able to assume both core- and conal-dominated “states” corresponding to its bright and weak modes. These circumstances appear to explain B0823+26’s B-mode X-ray bright/core-dominated radio emission or Q-mode X-ray faint/conal radio emission—and why the IP is X-ray quiet in both modes. (6) These same considerations applied to B0943+10 may explain why its brighter radio mode was conal and X-ray quiet, while the weaker one was X-ray bright—because its peripheral sightline would miss most core radiation.

*Unified Astronomy Thesaurus concepts:* Pulsars (1306); Polarimetry (1278); Nonthermal radiation sources (1119); Proper motions (1295)

## 1. Introduction

Pulsar B0823+26 (nee AP 0823) was one of the very first pulsars to be discovered by the then Arecibo Ionospheric Observatory (Craft et al. 1968), and has been an object of intensive study by astronomers over the last half century. The early discovery (Backer 1973) of an interpulse (IP) some 180° from the pulsar’s main pulse (MP) has led to the widespread belief (e.g., Hankins & Fowler 1986) that B0823+26’s magnetic axis is perpendicular to its rotation axis such that we catch a glimpse of both magnetic poles. The MP profile was also found (Backer 1973) to be followed some 30° later by a postcursor (PC), a feature seen in some pulsars that is both unusual and not yet well understood (Basu et al. 2015) in terms of the core/double-cone structure most rotation-powered pulsars show.

From the start, it was well known to Arecibo observers that B0823+26 was occasionally undetectable. However, this behavior was long attributed to especially deep scintillation, perhaps associated with its close proximity to Earth. Only in recent years was it discovered (Young et al. 2012) that the pulsar’s “weak” intervals appeared to be long nulls, with both bright and weak intervals sustained on timescales of hours such that the pulsar was undetectable for some 20% ± 10% of the time. Then, in a second surprise, Sobey et al. (2015) used the Low Frequency Array to show that the pulsar’s “null” intervals were actually a quiescent (Q or weak) emission mode—one comprised of sporadic weak pulses that on average, produced an aggregate emission level of about 1% that of the usual bright (B or strong) mode over a wide section of the radio spectrum.

This mode-switching property made B0823+26, already a known source of X-rays (Becker et al. 2004), an excellent candidate for investigating the possibility of its high-energy emission switching in tandem with its energetically insignificant radio emission.

The switch was spectacularly confirmed by the recent simultaneous radio/X-ray campaign conducted by the *XMM-Newton* satellite observatory together with the Giant Metrewave Radio Telescope (GMRT) and Low Frequency Array instruments (Hermsen et al. 2018). Remarkably, the project revealed an almost proportionate relationship between the X-ray and radio emissivity: strong X-rays are detected during the radio B mode, and the X-rays diminish by an order of magnitude or more to an undetectable level during Q-mode intervals. The X-ray emission appeared to be strongly pulsed and was argued probably to be of thermal origin and hence originating on the surface of the neutron star. However, the emission exhibited two unexpected features. First that the pulse cycle had only one peak, and second that this peak appeared delayed with respect to the radio emission’s MP, the presumed location of the magnetic pole. The GMRT radio observations used in the Hermsen et al. campaign have now been analyzed by Basu & Mitra (2019) and provide a number of interesting results.

The long-term radio/X-ray correlation over hours and across the various radio profile components therefore raises many questions of interpretation. While there is little doubt about the synchronous mode switch, underlined by a brief apparition of B-mode-like emission switching on suddenly at all wavelengths within a long Q-mode observation (Hermsen et al. 2018), the

switch back to the Q-mode was more gradual and flickering at both high and low energies, accompanied by changes in the radio profile across its components—a feature not seen in other radio mode-switching pulsars. Furthermore, this X-ray emission within the Q mode, and possibly that in the B mode generally, appears to evolve following their onsets.

This exceptional behavior raises the need for a more comprehensive understanding of pulsar B0823+26’s radio emission. Therefore we requested and received leave to use the Arecibo radio telescope to make new observations of pulsar B0823+26, mainly at 327 MHz (*P* band) but also at 1.4 GHz (*L* band). Most of these observations were scheduled in the period just before and after Hurricane Maria devastated Puerto Rico on 2017 September 20 (MJD 58016) and damaged the observatory. Indeed, the observation on MJD 58064 was one of the very first after Arecibo resumed limited operations—and it demonstrated that the reflector alignments were not critically damaged.

These observations were not conducted simultaneously with any X-ray observatory. Nonetheless, the program is extensive and represents a unique set of Arecibo rise-to-set observations. Through their analysis we have attempted here to clarify the nature of this pulsar’s radio modes, its modal transitions, and the subtle interactions between its components.

This first paper is organized as follows: the Arecibo observations are described in Section 1, Section 2 provides a review of B0823+26’s characteristics, Sections 3 and 4 deal with the bright and quiet-mode profiles while Section 5 explores the quantitative geometry, Section 6 considers possible physical interpretations, and Section 7 provides a summary of our conclusions.

## 2. Pulsar B0823+26 Prologue

Our new discoveries are based on a wealth of earlier studies of pulsar B0823+26, and a short review of these is pertinent to interpreting the star’s emission.

1. The timing properties of the pulsar are wholly typical of the older pulsar population, positioning it in the heart of the  $P-\dot{P}$  diagram. Its rotation period  $P$  is 0.531 s, and inferred age, spindown energy, and surface magnetic field strength are 0.95 Myr,  $4.5 \times 10^{32}$  erg s<sup>-1</sup>, and  $0.95 \times 10^{12}$  G. A principal factor in the discovery of its pulsed X-ray emission (Hermsen et al. 2018) is that it is one of the closest pulsars to Earth at only some 300 pc.
2. The pulse-component separations in the bright mode are well studied and bear strongly on the emission geometry. The MP-IP spacing is close to 180° and is independent of frequency, suggesting that the IP comes from the second magnetic pole. The PC trails the MP by about 30° and had been thought to have a possible weak frequency dependence (Hankins & Fowler 1986); however, Basu et al. (2015) showed that the apparent shift is due to a spectral change in its configuration.
3. The polarization position angle (PPA) can be tracked over a large part of the pulsar’s rotation cycle and is very well fitted with the rotating-vector model (RVM; Radhakrishnan & Cooke 1969; Komesaroff 1970) showing that the magnetic colatitude  $\alpha$  is close to 90° and suggesting that the sightline impact angle  $\beta$  is positive and only a few degrees. It also positions the PPA inflection point ( $\varphi_0$ ) as

lagging the center of the MP by only about 1° (Everett & Weisberg 2001, and references therein).

4. The B-mode MP appears well identified as mainly core emission—that is, having a core-single ( $S_1$ ) profile. Its 1 GHz half-power component width is very close to that of the  $3.38^\circ$  angular diameter of the pulsar’s polar cap [ $2.45 P^{-1/2}/\sin \alpha$ ] as discussed in Rankin (1993a, 1993b), and it often exhibits a small but consistent positive/negative antisymmetric circular polarization. Furthermore, the fiducial MP PPA exhibits a close orthogonal alignment with the star’s proper-motion (PM) direction of  $146^\circ \pm 1^\circ$  (Lyne et al. 1982) arguing strongly that the later emission of the core is polarized at right angles to the emitting  $B$  field and thus represents the extraordinary (X) propagation mode—this is seemingly another defining characteristic of core emission (Rankin 2007, 2015).
5. Finally, the pulsar seems to be another example of the predominant correlation between antisymmetric Stokes  $V$  signatures and the sense of the PPA traverse in core components (Radhakrishnan & Rankin 1990). Especially at low frequency, we see LHC/RHC in the core along with a positive-going (clockwise) PPA traverse.
6. In addition to this core emission, the B-mode MP profile exhibits weak outlier features both before and after the core peak (difficult to see in average profiles), suggestive of a conal outrider structure. This was noted by Rankin & Rathnasree (1995).
7. In the recently discovered Q mode, Sobey et al. (2015) detected only the MP, finding it almost coincident with the B-mode MP and perhaps narrower. Basu & Mitra (2019) also detected the Q-mode PC and found that its MP showed considerable evolution with a width almost 50% wider and resembling a barely resolved double shape.

In this paper we will take advantage of all these earlier results and build on them in several ways.

## 3. The Bright-mode Profile

This pulsar’s profiles are shown in Figures 1 and 2 at 1.2 GHz and 326 MHz, respectively. The profiles are plotted in total power and then replotted at 25 times amplitude to show the detailed polarization behaviors in the PC and IP features. Figure 3 also shows the profile at 4.6 GHz with a 100 times scaleup. The RVM curves (dashed-dotted red) are absolute in the sense that they have been Faraday-derotated (Curtin et al. 2020) to infinite frequency and take their origins along the pulsar’s PM direction (cyan).<sup>5</sup> The PPAs are plotted (black) along with the orthogonal angle (blue). Therefore, it is clear that most of the trailing MP emission as well as that of the PC is orthogonal and thus the X physical mode; however, that in the leading region is more mixed with the leading portion being ordinary (O) propagation-mode dominated. This parallels what was found by Rankin & Rathnasree (1995), except that they were not yet able to associate the PPM/secondary polarization mode (SPM) with the X/O modes.

<sup>5</sup> Our 1.4 GHz polarimetry indicates a smaller peak fiducial PPA than 98° (Morris et al. 1979), but measurement uncertainties prevent a precise comparison. We have therefore applied small ( $10^\circ$ – $15^\circ$ ) rotations so as to reference our polarimetry to the well-determined PM direction.

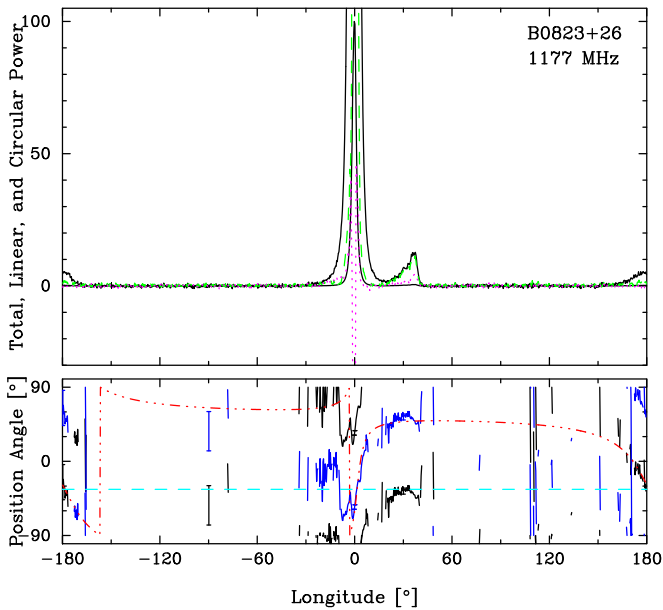


**Figure 1.** Upper panel: the total power (Stokes  $I$ ) profile at 1.2 GHz from modified Julian date (hereafter MJD) 55522 is first plotted full scale (thick black); then the total power (thin black), total linear polarization ( $L = \sqrt{Q^2 + U^2}$ ; dashed green) and circular polarization (Stokes  $V$ , defined as left-hand–right-hand circular polarization; dotted magenta) are replotted at  $25\times$  to show the PC and IP clearly. A box at  $-150^\circ$  giving the resolution ( $0.3^\circ$ ) and a three off-pulse-noise standard-deviation deflection is not seen here because the signal-to-noise ratio is too large. Lower panel: the absolute, Faraday-derotated, PPA  $[\frac{1}{2}\tan^{-1}(U/Q)]$ , and its orthogonal PPA is shown (blue), both with occasional  $2\sigma$  error bars. The RVM curve (red, dashed–dotted) is also given along with the orientation of the pulsar’s PM (cyan).

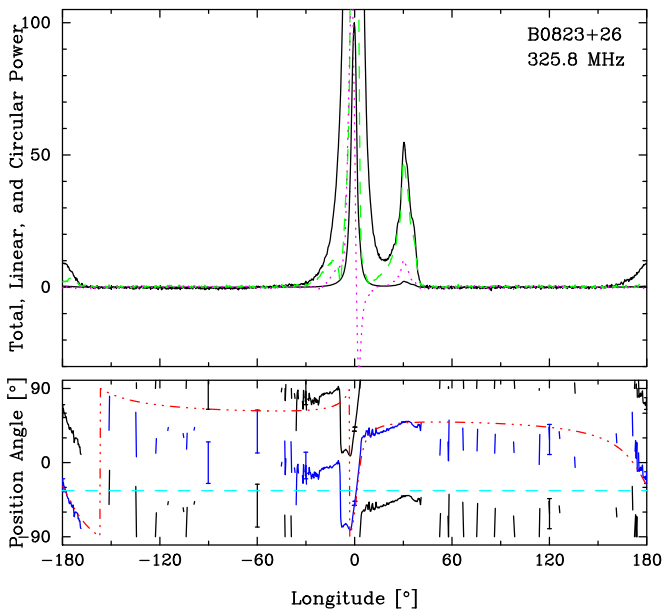


**Figure 2.** Polarization profile at 326 MHz on MJD 57915 after Figure 1.

### 3.1. MP Polarization in the B mode

Figure 4 shows the MP region of the observations in Figures 1 and 2 with a scale multiplier of only 2 to better show the linear and circular polarization. Note that the aggregate linear polarization is not centered within the MP total power profile, rather it trails the core peak by about  $0.5^\circ$ . Also, the 327 MHz profile shows the  $\pm$  antisymmetric circular

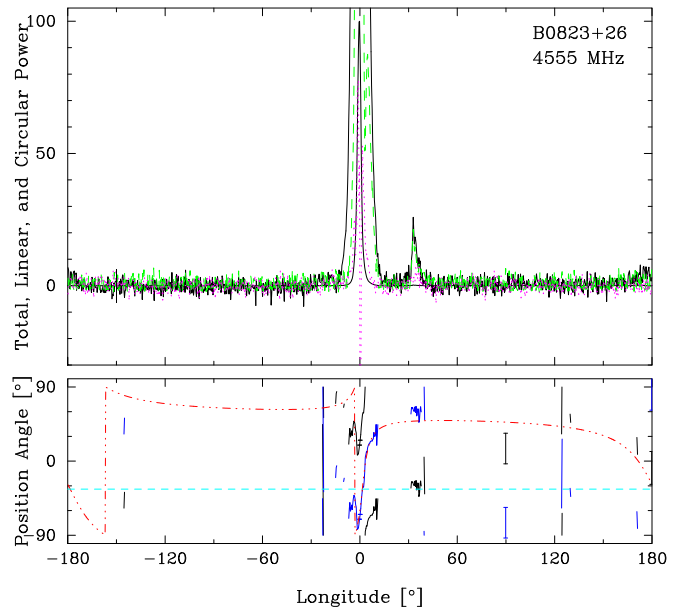


**Figure 3.** Polarization profile at 4.6 GHz on MJD 57292 after Figure 1. Here the scale multiplier is 100 to show the weak PC and barely discernible IP.

polarization signature seen consistently below 1 GHz (e.g., Gould & Lyne 1998), whereas it is more complex and variable at higher frequencies.<sup>6</sup>

Various aspects of pulsar B0823+26’s bright-mode emission were explored by Rankin & Rathnasree (1995). In particular, the two polarization modes were distinguished and three-way mode-segregated profiles (see the Deshpande & Rankin 2001 Appendix) were computed for study. While the pulsar’s PPA traverse conforms to the RVM more closely than most pulsars, this analysis showed that both polarization modes contribute significant power to the MP core feature, especially in its depolarized leading region. Also, the SPM emission showed a conal “outliner” structure at 430 MHz that we have confirmed by peak histogram analysis (Olszanski et al. 2019) as an outer cone.

Our high-resolution MP polarization displayed in Figure 5 provides evidence of these outer features as well as inner ones. The core emission shows the steep X-mode PPA traverse under the slightly delayed highly polarized MP feature as well as a depolarized mixed-mode region preceding it. Regions of what seem to be inner cone O-mode emission are perceptible on each side of the core as well as “shadows” further out produced by the outer conal emission as we will treat in detail in a further paper.

### 3.2. PC Properties

Only a few pulsars exhibit PC components, and so far we have no satisfactory explanation for either their existence or the geometry/physics of their emission. Basu et al. (2015) studied the phenomenon in the pulsars with known features, including

<sup>6</sup> The pulsar’s single-pulse emissions are highly linearly polarized with the X propagation mode dominating in the trailing MP regions and the O mode in the leading region. The circular polarization in single pulses is also much higher than its average with LHC predominating under the early part of the MP and RHC thereafter. It therefore appears that the O mode tends to be positively circularly polarized, the X mode negatively, and both  $L$  and  $V$  experience substantial depolarization within the average MP profile overall. We will discuss this further in subsequent papers.

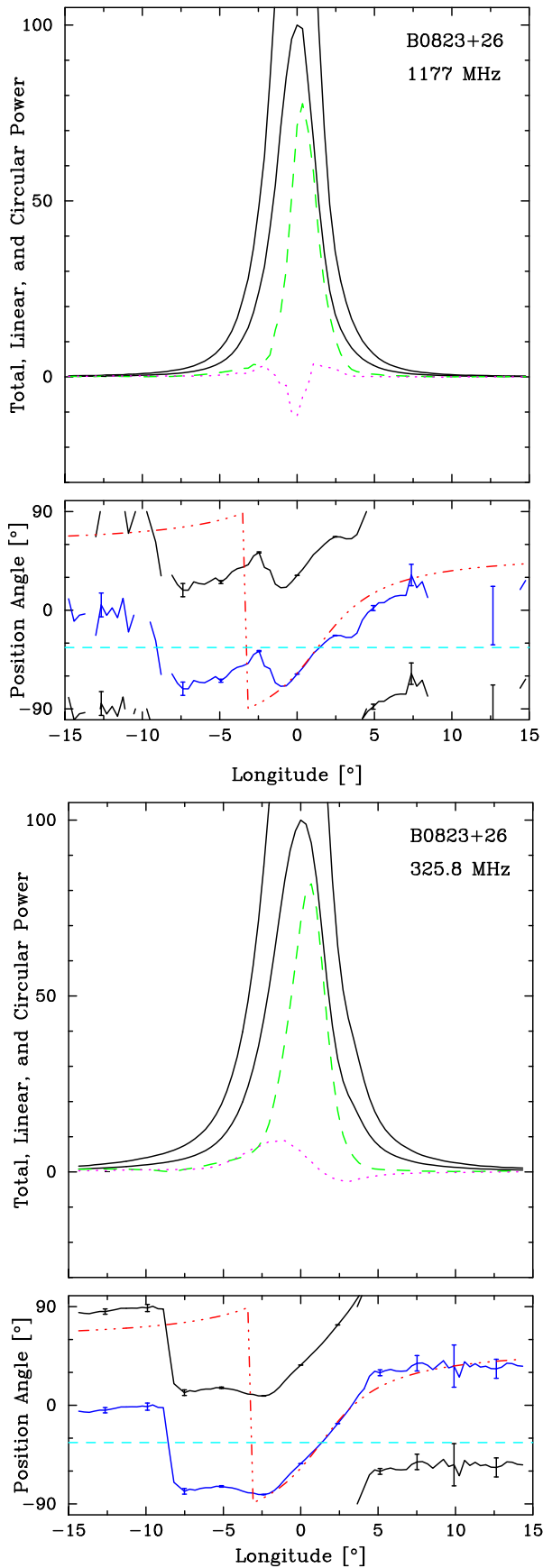


**Figure 4.** MP profiles at 1.2 GHz and 326 MHz after Figures 1 and 2. Here the scale multiplier is 2.

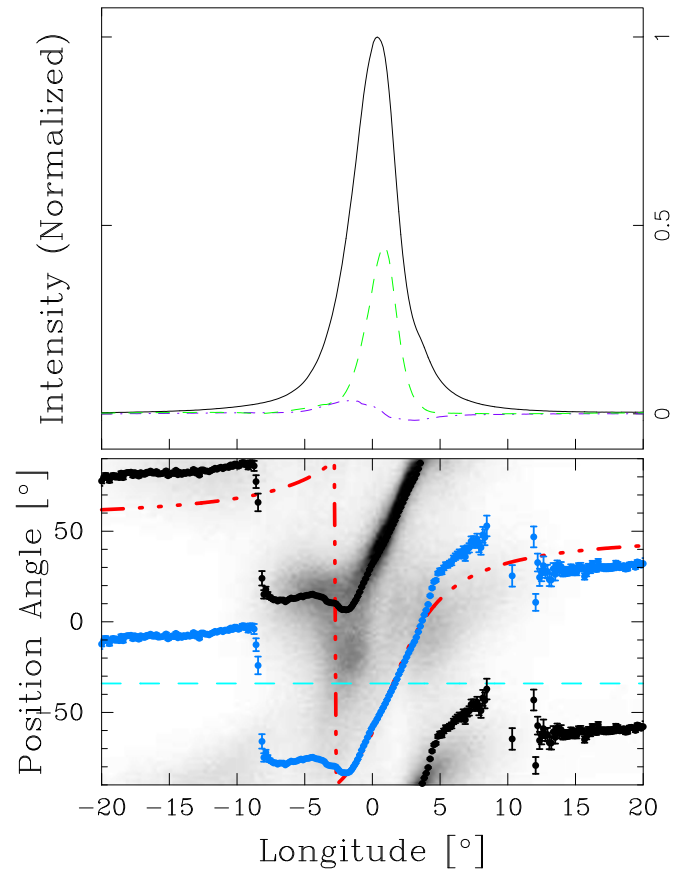


**Figure 5.** High-resolution MJD 58509 MP profile. The upper panel shows the average profile around the MP region, while the lower panel shows the single-pulse PPA distribution and average (black) along with the orthogonal PPA track (blue). The RVM curves and PM direction are shown as in Figure 1.

B0823+26, but were unable to understand how or where they are emitted.

Pre-/PCs tend to have steep spectra and be highly linearly polarized as is the one in B0823+26 (e.g., Figures 1–3). Here we can also see that the peaks of the 1.4 and 0.327 GHz PC features fall at different longitudes relative to the MP peak; however, Basu et al. (2015) showed that the PC has several components with differing spectra such that the overall feature is stationary. The high-resolution profile in Figure 6 shows clearly that its PPA traverse falls close to the RVM curve associated with the primary polarization (X) mode. Its 327 MHz structure also suggests the presence of several components that seem to mirror the conal configuration of the MP—an issue we will discuss further in subsequent papers.

### 3.3. IP Profile Properties

The IP is between 50 and 100 times weaker than the MP. As seen in the high-resolution profile in Figure 7 it falls close to  $180^\circ$  from the MP PPA inflection point and has a larger half-power width of about  $10^\circ$ . It has an asymmetric, possibly unresolved double, shape with a depolarized leading region and only a modest level of linear polarization thereafter. Its PPA squares well with the RVM showing mainly X-mode emission at 327 MHz and a mix of X and O at 1.4 GHz. Its width is too broad to be a core component, and were  $\alpha$  as far from  $90^\circ$  as is measured ( $81^\circ$  by Everett & Weisberg 2001), we can question

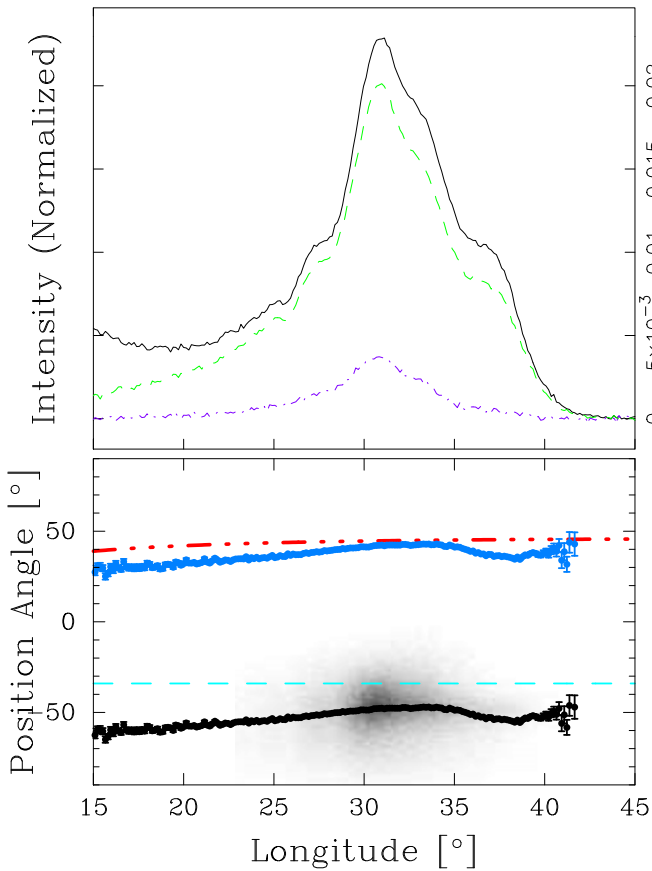


**Figure 6.** High-resolution 327 MHz PC profile after Figure 5. The upper panel shows the average profile around the PC region, while the lower panel shows the single-pulse PPA distribution and average (black) along with the orthogonal PPA track (blue).

why we can see it at all. Its properties suggest that it is conal, but were it to have an outer cone geometry, its viewing (impact) angle  $\beta_{\text{IP}}$  would need to be about  $5^\circ$ —which in turn would argue for an  $\alpha$  value closer to  $90^\circ$ . That it shows little frequency evolution is also suggestive of a conal single configuration.

#### 4. The Quiet-mode Profile

In our many observations, we were fortunate to record three rise-to-set observations (two at 327 MHz, one at 1.4 GHz) of this mode. While the emission is indeed very weak, (on average 100 times weaker than the bright mode), and thus easily corrupted by radio-frequency interference (RFI), we have been able to distinguish the pulsar’s single pulses from the RFI to construct satisfactory polarized profiles. Polarization displays of the MP-PC region are given in Figures 8 and 9. The upper panels show the full rotation cycle and the lower ones the MP-PC region. In these Q-mode profiles we see clearly that the PC is emitted in this mode and that the IP is only detected at the lower frequency. We also find that the Q mode’s PC shifts closer to the MP’s peak by about  $3^\circ$ , and we believe this is caused by a change in location of the MP’s peak intensity as we will show below.

##### 4.1. MP Component Structure and Polarization

Figures 8 and 9 show immediately that the MP profile is very different in the weak mode: it shows two features at both

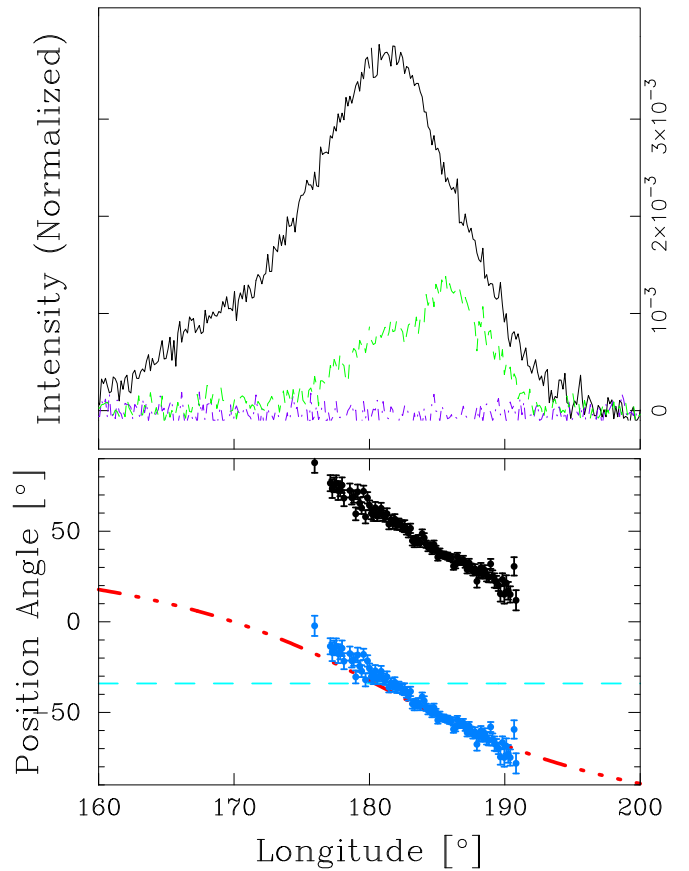


**Figure 7.** High-resolution 327 MHz IP profile after Figure 5. The upper panel shows the average profile around the IP region, while the lower panel shows the average (black) and orthogonal (blue) PPA tracks.

frequencies and has a substantially larger width. The 1.4 GHz profile is better resolved than the lower frequency, and both its shape and the circular polarization suggest the presence of some weak core emission filling the center at 327 MHz.

Another prominent difference between the weak- and strong-mode MPs is their linear polarization. We saw above (Figures 1–3) that the MP primarily shows X-mode emission, apart from a mode-mixed region on its leading edge. By contrast, the weak mode MP emission is mostly ordinary (O) mode as can be seen in Figures 8 and 9. The 1.4 GHz linear polarization is slight; however, at 327 MHz the linear PPA closely tracks the O-mode RVM apart from a narrow region at the very center where some residual X-mode core radiation may be accruing to the profile.

Most prominently, we see that the MP profiles of the weak mode are very different than those of the strong mode. Each has two unresolved features or components and their widths, measured between the half-power points of the two components, are substantially larger than that of the bright-mode MP. Moreover, they are O-mode dominated, unlike their B-mode counterparts, and their fractional linear polarization is smaller than in the B mode suggesting more mode mixing. All these properties argue strongly for interpreting the weak-mode MP as a conal double structure.

##### 4.2. PC Structure and Polarization

Figures 8 and 9 also show the weak mode PC feature. At both frequencies we see that it follows the absolute X-mode

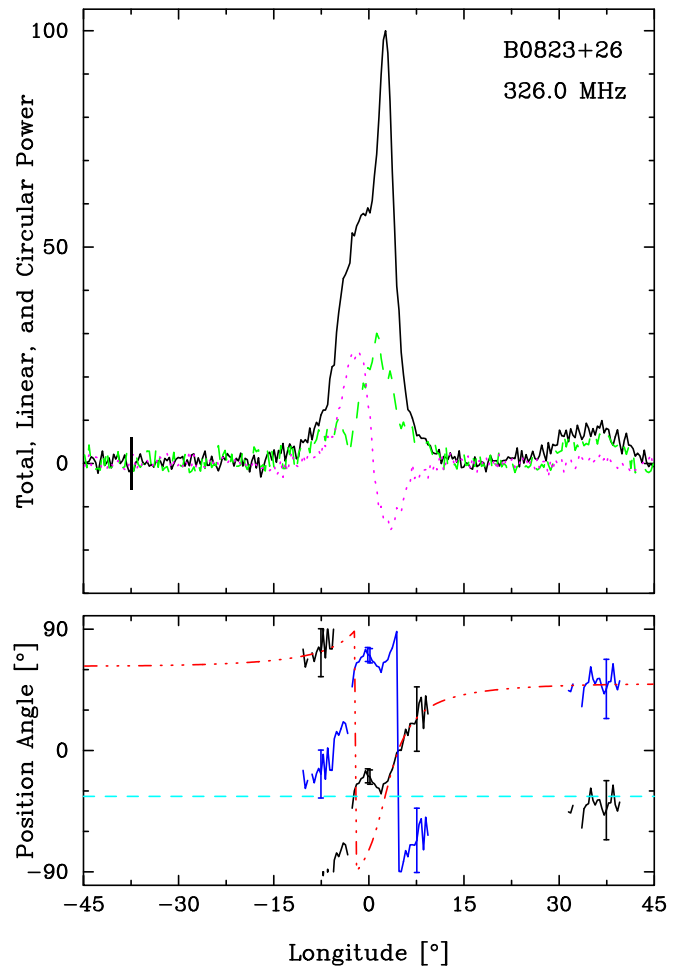
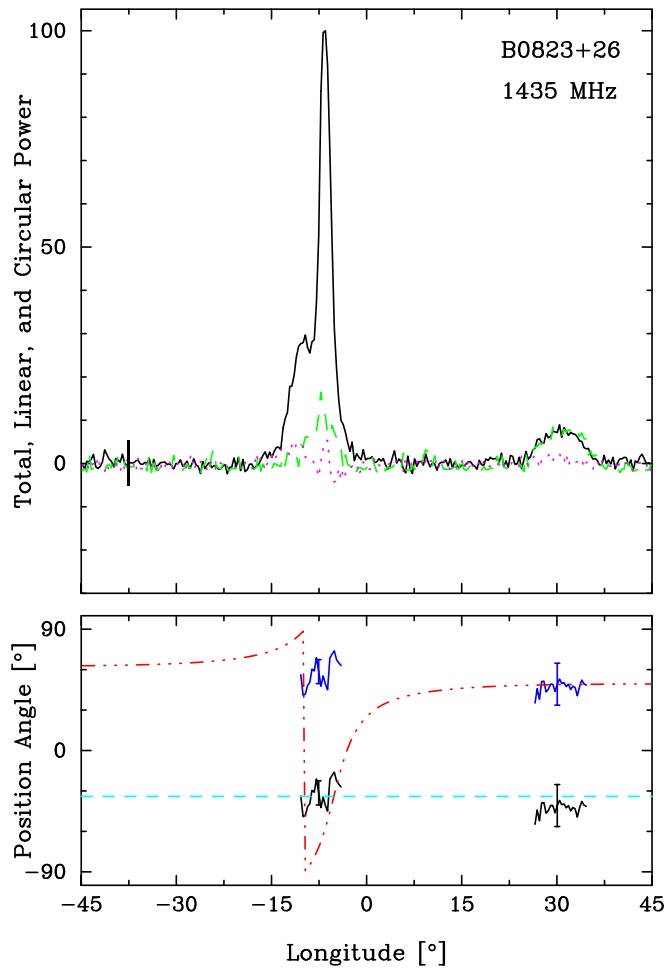
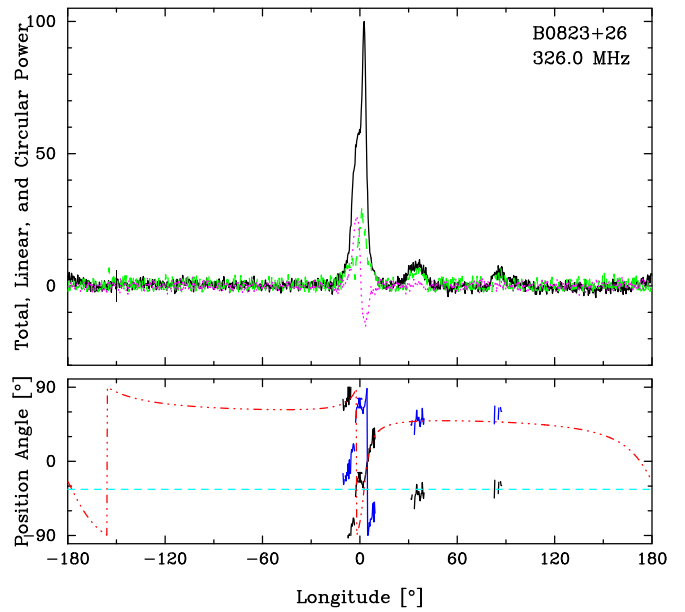
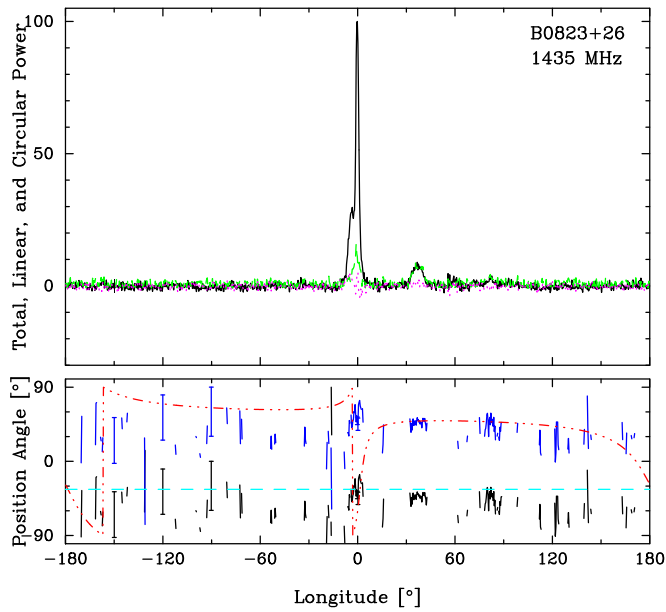


**Figure 8.** Full period (upper) and MP/PC (lower) profiles at 1435 MHz after Figures 1 and 4 showing the Q mode in the rise-to-set MJD 58064 observation. Note the presence of the PC although the IP was not detected in this observation. The MP here again has two unresolved components with the fractional linear stronger in the trailing region. The broad weak emission feature at about  $+80^\circ$  is also seen consistently in our Q-mode observations.

**Figure 9.** Full period (upper) and MP/PC (lower) profiles at 327 MHz after Figures 1 and 4 showing the Q mode in the rise-to-set MJD 58205 observation. Note both the PC and the IP in this observation. The fractional linear of the two-lobed MP is stronger in the trailing region, and a strong  $+/-$  antisymmetric circular signature is seen. Note also that the PPA follows the O mode on both edges of the profile with some complexity near the positive V peak—a very different behavior than in the bright mode.

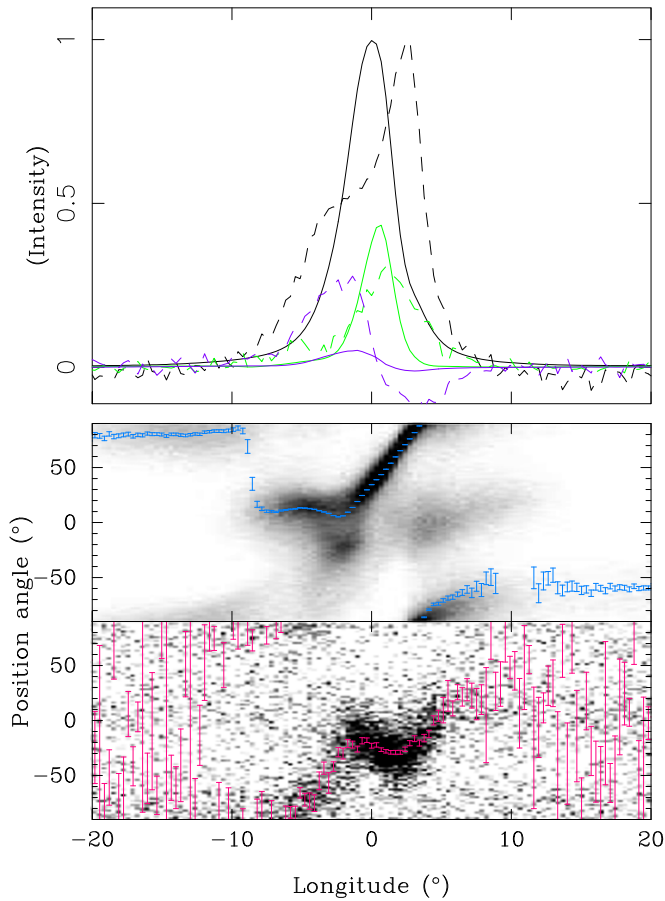


**Figure 10.** Display showing the alignment between the 327 MHz bright-mode observation on MJD 57900 (solid curves) and the weak mode (dashed) on MJD 57914. The total power (black), linear (green), and circular (blue) of the two observations are shown in the top panel, and the PPA densities in the lower two panels, respectively. The alignment was determined by timing between the observations. Note that the bright-mode profile is nearly centered within the broader weak mode one and that the linear peaks nearly coincide. Note also that the PPA traverses nearly coincide at the profile centers but tend to be orthogonal elsewhere.

PPAs of the RVM curve and is highly linearly polarized at both bands. This PC polarization is fascinating and significant because the Q-mode PC remains X-mode dominated, despite the X-mode radiation largely disappearing from the MP.

#### 4.3. New Quiet-mode Intrapulse Emission

Furthermore, it is apparent at both frequencies that a weak region of emission lies between the MP and IP. This inter-pulse (IIP) is unlikely to be RFI, as it is present in all our weak mode observations, and its polarization follows the RVM curve, along with it being X-mode emission. As far as can be discerned, the bright mode does not exhibit an IIP, suggesting it is a feature unique to the Q mode. Three of the five emission regions (MP core, PC, and IIP) exhibit X-mode polarization while two (IP and MP cone) do not. It is interesting to see X-mode emission being associated with low lying core emission, and high altitude PC and IIP emission.

#### 4.4. B- and Q-mode Profile Alignment

From an analysis of the pulsar’s timing, as well as a study of a B- to Q-mode transition, we estimated a profile-peak offset of  $3^\circ$  between the B and Q modes, and this agrees quite closely with

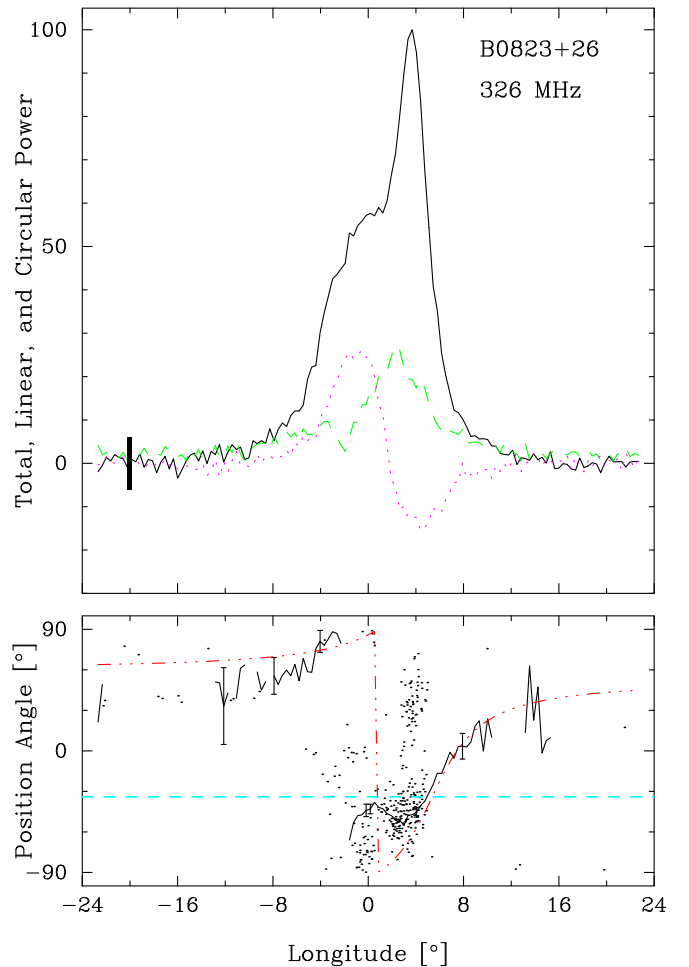


**Figure 11.** Quiet-mode MP profile after Figure 5 from MJD 58205. The upper panel shows the average profile, while the lower panel shows the average PPA track along with the distribution of single-pulse position angles.

the estimate of Sobey et al. (2015). Figure 10 shows the overlaid profiles together with their polarization, and we see that the Q-mode distinguishes itself from the B mode through a lack of core emission. In fact, the features seen in the Q-mode profile (Figure 9 at  $-8^\circ$ ,  $-2.5^\circ$ ,  $+2.5^\circ$ , and  $+8^\circ$ , see also Figure 11) agree closely with what seems to be an inner/outer conal pair in the B mode. We also see that in this alignment, the PCs of both modes coincide. This would explain the previously mentioned shift of the PC. In the Q mode, the trailing inner cone becomes the dominant component resulting in a shift of the PC toward the MP. In short, neither the conal components nor the PC feature shifts in location, suggesting that the overall emission is originating from similar regions and heights in both modes.

## 5. Exploring B0823+26’s Emission Geometry

The previous sections provide a strong basis for interpreting the profile structure of pulsar B0823+26.

1. In the B mode the MP is dominated by core emission but conal emission is perceptible around it, the IP is mainly conal, and the PC remains a mystery, but has a total width very similar to that of the conal emission within the MP.
2. The Q-mode profile seems to be a weaker version of the B mode, but stripped of almost all core emission. The MP profile is broader and has what appears to be an inner

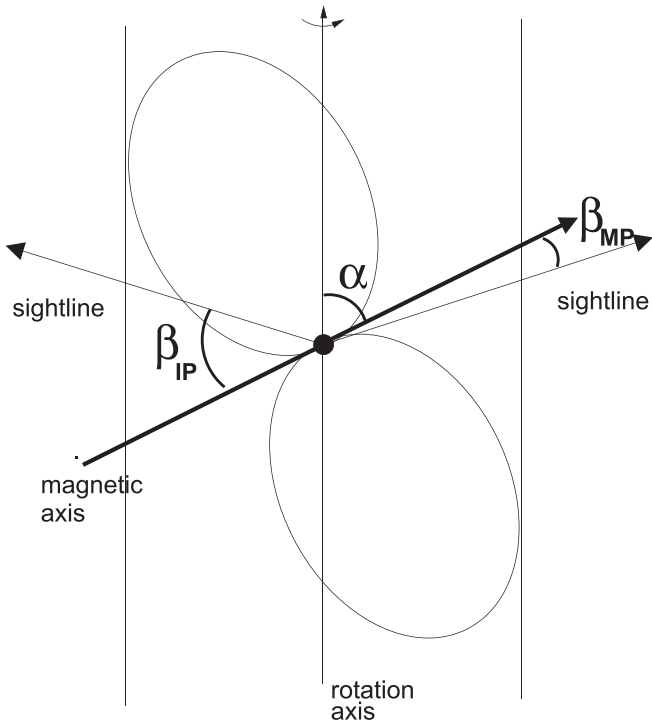


**Figure 12.** Sightlines with respect to the MP and IP, with both  $\beta_{IP}$  and  $\beta_{MP}$  assumed positive, as suggested by B0823+26’s PPA traverse.

conal double profile, and both the PC and MP are present at the same profile positions.

3. In assuming the Everett & Weisberg (2001) geometry with the inflection point taken at the pulsar’s PM direction, we have found that it gives a very close fit to the pulsar’s observed PPA traverse.

In this section we will explore various aspects of the quantitative geometry in order to examine whether the qualitative conclusions above hold up quantitatively.

### 5.1. Core/Double-cone Beam Dimensions

In B0823+26’s B mode, we can accurately determine the properties of the bright MP core component relative to the other components and the PPA inflection point; however, measuring the dimensions of the underlying conal components is difficult because they are so weak. In the Q mode, the apparent conal structure of the MP is readily measured, but any residual core emission within it is conflated beyond recognition.

In order to distinguish these profile features, we need to resort to methods of individual pulse analysis; however, here we chose to concentrate on profile analyses and defer the (exceedingly interesting!!) pulse dynamics to a later paper in this series. Nonetheless, some of what we need here has already been published in Rankin & Rathnasree (1995); Weltevrede et al. (2006; 2007); Basu & Mitra (2019); and Olszanski et al. (2019), where the well-known B-mode 5-*P* modulation reveals conal activity.

Our measured and estimated widths and spacings of the profiles are given in Table 1. The MP, IP, and PC widths are all well determined at 327 MHz, and the MP and PC are as well at 1.4 GHz. The conal parts of the MP are more difficult, and we have estimated them using the single-pulse analyses above.

**Table 1**  
Double-cone Geometry Model for B0823+26

Band (MHz)	$w_i$ (°)	$\rho_i$ (°)	$w_o$ (°)	$\rho_o$ (°)	$h_i$ (km)	$h_o$ (km)
<b>Bright MP</b>						
1400	~9	5.4	~14	7.6	103	205
430	...	...	~16	8.5	...	258
327	9.3	5.5	~17	9.0	108	287
<b>Bright PC</b>						
327–1400	...	...	14.5	7.8	...	217
<b>Bright IP</b>						
1400	...	...	12.5	8.0	...	226
327	...	...	14.0	8.6	...	261
<b>Weak MP</b>						
1400	~8	5.0	...	...	88	...
327	9.5	5.6	...	...	111	...
<b>Weak PC</b>						
327–1400	...	...	14.5	7.8	...	217
<b>Weak IP</b>						
1400	...	...	?	...	...	...
327	...	...	?	...	...	...

**Note.**  $w_i$  ( $w_o$ ) are the outside half-power widths of the inner (outer) cone or conal component pair.  $\rho_i$  ( $\rho_o$ ) are the outside half-power beam radii, and  $h_i$  ( $h_o$ ) are the characteristic emission heights.

The interpolated 1 GHz B-mode MP core has a 3.38° width, and as in Rankin (1993a) this supports an  $\alpha$  value of close to 84° using that paper’s Equation (1). Two rough MP cones can be discerned at 327 MHz and one at 1.4 GHz. Their estimated dimensions are given in Table 1, and the conal radii are computed using Everett & Weisberg’s (2001)  $\beta_{MP}$  of 3° and Equation (4). The characteristic emission heights then come from Equation (5).

The conal beam radii can be compared with what is expected for a pulsar of B0823+26’s period—or, what is the same, the estimated emission heights should fall around 120 km for inner cones and 220 km at 1 GHz (or larger at lower frequencies) for outer cones. Within the limits of our estimates, this seems to be the case. Also noted is that a  $\beta_{IP}$  value of about 4.5° seemed to best account for the outer cone geometry of the IP.<sup>7</sup>

### 5.2. Aberration/Retardation Emission Heights

As noted above, Everett & Weisberg’s (2001) PPA fit shows that the RVM inflection point falls about 1° after the MP peak. This can be used to obtain an aberration/retardation measurement of the physical emission height of the core radiation (Blaskiewicz et al. 1991 as corrected by Dyks et al. 2004) as well as rough estimates of the conal emission heights. The longitudes in Table 2 take the PPA inflection point as their reference.

### 5.3. Implications for the Geometry of the Pulsar and Observer

An understanding of the B mode’s integrated polarization properties, especially the correct assessment of the PPA traverse is important because it makes it possible to fix the common viewing geometry of both the pulsar’s B mode and its much weaker Q-mode.

In any pulsar where the magnetic and rotation axes are nearly perpendicular the precise magnitude and sign of the respective

<sup>7</sup> We do not, of course, know just where or how the PC is emitted; however, it has too large a width to be an inner cone, so we have included its width in the table and processed it as an outer cone to emphasize that it has dimensions similar to the conal parts of the MP in both modes.

**Table 2**  
B-mode Aberration/Retardation Heights for Pulsar B0823+26

Component	Frequency (GHz)	$\phi_l$ ( $^\circ$ )	$\phi_t$ ( $^\circ$ )	$\phi_c$ ( $^\circ$ )	$r$ (km)
Core	0.33	-2.5	1.4	-0.53	116
Inner cone	0.33	-2.7	1.5	-0.61	133
Outer cone	0.33	-8.8	6.6	-1.1	243
Core	1.4	-2.0	1.0	-0.53	117
Inner cone	1.4	-2.5	1.5	-0.61	135

**Note.**  $\phi_l$  ( $\phi_t$ ) are the leading (trailing) longitude positions of the components. For the core, we take this as the half-power point, and for the cones the component peak positions are estimated.  $\phi_c = (\phi_l + \phi_t)/2$  and  $r = -c\phi_c P/2/360$ .

impact angles  $\beta_{\text{MP,IP}}$  and the inclination  $\alpha$  itself become very important for the interpretation of the observed emission. For B0823+26 there seems little doubt that  $\alpha$  is close to  $90^\circ$  and that  $\beta_{\text{MP}}$ , though positive, is not such that  $\alpha + \beta_{\text{MP}}$  exceeds  $90^\circ$ .

A consequence of this is that the observed open field line at the fiducial point of the MP will be viewed close to the pulsar surface in a region that is conventionally positively charged, while that of the IP will be at a much greater altitude in a negatively charged region. It is a matter of simple geometry in Figure 12 that

$$\beta_{\text{MP}} + \beta_{\text{IP}} = 2(90^\circ - \alpha), \quad (1)$$

so that if we take the values  $\alpha = 81^\circ$  and  $\beta_{\text{MP}} = 3^\circ$  given by Everett & Weisberg (2001)—albeit with significant error bars—then  $\beta_{\text{IP}} = 15^\circ$ , a value unlikely to make the IP detectable. Taking the more plausible  $\beta_{\text{IP}} \approx 5^\circ$  suggested in the previous subsection, then we need an inclination  $\alpha$  nearer to  $86^\circ$ , giving the very small  $\beta_{\text{MP}} \approx 3^\circ$ . Thus, assuming we are dealing with an axisymmetric magnetic field, there is little doubt that its axis is almost perfectly orthogonal to the rotation axis and our chance line of sight just squeezes between the axis and the star’s equator.

#### 5.4. Magnetospheric Geometry

Our program of multifrequency Arecibo B0823+26 observations has confirmed the basic radio features of its B-mode emission. In this mode the pulsar has three components: an MP, a PC, and an IP. The last of these located  $180^\circ$  from the MP at all frequencies support the widespread assumption that the object is a two-pole interpulsar. As reported by Hankins & Fowler (1986), the location of the PC peak varies with a frequency between  $30^\circ$  and  $40^\circ$  as seen in Figures 1–3. We support the view of Basu et al. (2015) that the PC has a two (or even three) component structure such that the primary feature gradually shifts with frequency toward a  $40^\circ$  separation.

The observed PPA traverse is compatible with the RVM, and we show that for both the MP and IP to be observable from Earth, the pulsar must have an inclination  $\alpha$  very close to  $90^\circ$  with our sightline of the MP lying tightly between the magnetic axis and the rotational equator (see Section 5.3). This has interesting implications for the contrasting physical regions we are observing at either pole. In the first-order model of a pulsar’s magnetosphere the electric fields parallel to the magnetic field lines are supposed to be screened. This results in “null” surfaces that divide regions of opposite charge sign,

and the intersection between these and the last closed field lines are thought to be the site of “outer gaps” (which may result in the production of nonthermal X-rays).

In near-aligned pulsars the outer gaps exist at high altitude and the pulsar’s surface polar gap is treated both observationally and theoretically as a separate region (see Figure 13 left). In the extreme geometry of B0823+26 this is no longer true (see Figure 13 right). While the null surfaces that azimuthally precede and follow the magnetic axis are still at a significant fraction of the light cylinder, the surface below the axis can only be a degree or two above the equator—implying a height of only 150 km. It must even lie at an angle below our sightline for the observed field line to be directed toward us, and there can be little doubt that that field line must originate in the core region of the polar cap.

The MP emission we observe must therefore come from a region where at its wings the field lines cross the null surface at a great altitude, while at the central longitudes the emitting field lines interact with a low-altitude outer gap—and this picture is confirmed by our observation that the MP peak leads the fiducial point by about  $1^\circ$  giving an aberration/retardation height of some 140 km. As argued in Section 3, the narrowness and polarization of the MP is strong evidence that this component is primarily core emission. However, two zones of secondary mode emission revealed by mode separation have a double profile form that has the dimensions of an outer conal radiation beam, in keeping with the rapid rise in the height of the null line at pulse longitudes away from the fiducial plane. Thus, while the polar cap defined by the last closed field lines is still roughly circular, the observed emission it generates is a hybrid of both core and conal.

In contrast, the region that we are viewing at the IP will be at a greater altitude and of opposite net charge sign to the MP. The relatively large  $\beta_{\text{IP}}$  implied by Equation (1) means that we are likely viewing outer cone emission at a height between 200 and 300 km (see Table 1). We cannot assume that core emission is simultaneously present at both poles because from our viewing angle it would not be detected. However, given the weak X-ray emission associated with the IP, its radiation is probably exclusively conal.

The location of the PC emission remains a conundrum. Because it follows the MP after only  $30^\circ$ – $40^\circ$  and is connected to it by an emission bridge it might be reasonable to assume that its emission lies on field lines connected to the polar cap. If so, Basu et al. (2015) estimate that they are placed at 6400 km. However, if the emission is linked to appropriate conal field lines the height must be much greater. Curiously, the PC itself appears to have a two- or three-component structure (see Figure 6), suggesting a one-to-one mapping to specific regions within the polar cap as defined in Table 1. This possibility will be pursued in the single-pulse analysis of a subsequent paper.

In the Q mode, and during its evolution from the B mode, the observing geometry clearly remains unchanged, and we see again all three components of the B mode, but at greatly reduced intensity. However, the MP profile is somewhat broader and exhibits an unresolved double form. Modeling it with the geometry of Rankin (1993a, 1993b) identifies it as an inner cone with the usual characteristic emission height of about 120 km. Thus, it appears that the Q mode is equivalent to the B mode, which gradually, in a flickering manner, loses its dominating core emission.

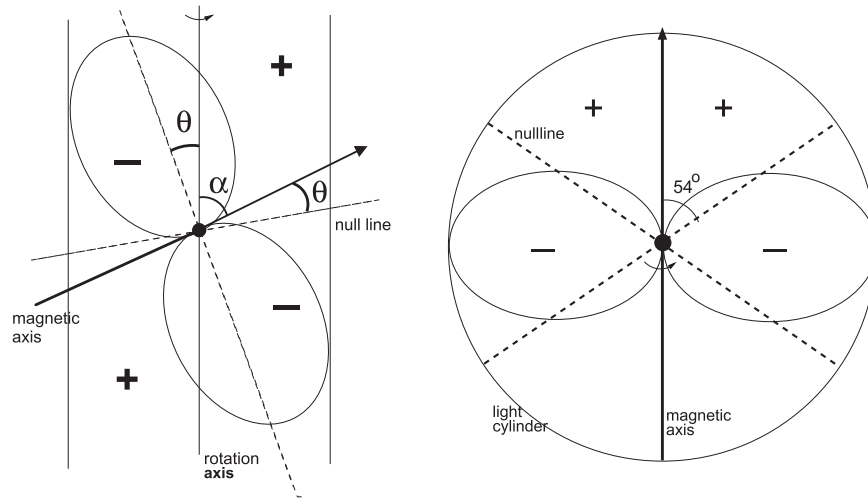


**Figure 13.** Left: the position of the null surfaces in the fiducial plane of a highly inclined pulsar, assuming a dipolar field. Note the small  $\theta$ , so that one null surface intersects the last closed field line close to the star. Right: null surfaces in the poloidal plane of the dipole with  $\alpha \approx 90^\circ$ . Note that the null line intersections are now at a significant proportion of the light cylinder radius

An intriguing aspect of the Q mode is the appearance of weak emission at a longitude of about  $+80^\circ$ , which we were able to identify clearly in the long Q-mode sequences at both frequencies.<sup>8</sup> This emission must occur at high altitudes, but its geometry is intriguing because to be so far from the MP it must be from upward moving particles on a field line close to the light cylinder turning strongly away from the MP. Strong aberration and retardation will shift its appearance to an earlier longitude. It is possible that this emission could be on the same field lines as the PC.

A puzzling feature of the X-ray results is that the peak of pulsed B-mode emission does not directly coincide with the radio MP but is shifted about  $75^\circ$  later. Hermsen et al. (2018) interpret this as a combination of two thermal sources located at the pole. However, we would suggest that only one of the sources is polar heating, the other being nonthermal X-rays coming from the same magnetosphere location as the weak radio emission found in the Q mode between PC and IP, indicating a physical connection to a common feature such as an active/dormant outer gap.

## 6. Core and Conal Plasma-generation Physics

The principal and exciting result of Hermsen et al. (2018) was that the X-ray emission of B0823+26 switched in tandem with the radio mode, and that the X-ray emission seemed largely thermal. This meant that the mode switch could be characterized by a dramatic change in the polar cap temperature. In this paper we have demonstrated that the radio mode change can equally well be seen as a turning on and off of core emission. It follows that the presence of core emission in a pulsar is an indicator of surface heating.

Timokhin & Harding (2015) argued that pulsars generate the electron-positron plasma needed for the emission in one of two pair-formation-front (PFF) configurations. For the younger, energetic part of the pulsar population, pairs are created at some 100 m above the polar cap in a central, uniform (1D) gap potential that produces copious backflow heating and thus

thermal X-rays—thus a 2D PFF, whereas for older pulsars the pair-formation front has a lower, annular shape and extends up along the conducting walls of the polar flux tube, thus becoming three-dimensional (cup shaped) with a 2D gap potential and greatly reduced backflow heating. Curvature radiation generates the pair plasma in both cases, dominating the inverse-Compton process. An approximate boundary line between the flat and cup-shaped pair-formation geometries—and thus pulsar populations—is plotted in the  $P-\dot{P}$  diagram of Figure 14, so that the more energetic pulsars are to the top left and those less so at the bottom right. Its dependence is  $\dot{P} = 4.29 \times 10^{-29} \rho P^{9/4}$ , where the field-line curvature is  $\rho = 9.2 \times 10^7 P^{1/2}$ , overall giving  $\dot{P} = 3.95 \times 10^{-15} P^{11/4}$ .

We emphasize in this context that pulsars with dominant core emission uniformly lie in the upper left part of the  $P-\dot{P}$  diagram above this boundary, whereas those with dominant conal emission lie to the lower right of the line. This boundary line seemingly divides the pulsar population between the younger stars whose radiation is core dominated and those older pulsars whose emission is mainly conal. In particular, B0823+26 itself lies close to the left of the boundary.

This division is fundamental to the core/double-cone beam model of Rankin (1993a, 1993b), where the several types of radio pulsar profile classes are defined. Pulsars with conal single ( $S_d$ ), double ( $D$ ) and five-component ( $M$ ) profiles fall below the boundary lines to the right, whereas those with core-single ( $S_r$ ) profiles are found to the upper left of the boundary. Those with triple ( $T$ ) profiles are found on both sides of the boundary, but divide roughly into core-dominated and conal-dominated groups, which are delineated by the boundary line. In the parlance of Rankin (1993a, 1993b), the division corresponds to an acceleration potential parameter  $B_{12}/P^2$  of about 2.5, which in turn represents and energy loss  $\dot{E}$  of  $10^{32.5}$  erg  $s^{-1}$ . B0823+26 falls just above these values with a  $B_{12}/P^2$  value of 3.44 and a  $\log_{10} \dot{E}$  of 32.66. This delineation also squares well with Weltevrede & Johnston’s (2008) observation that high-energy pulsars have distinct properties and Basu et al.’s (2016) demonstration that conal drifting occurs only for pulsars with  $\dot{E}$  less than about  $10^{32}$  erg  $s^{-1}$ .

We therefore propose a scenario in which the bright and quiet modes of B0823+26 represent largely different polar cap

<sup>8</sup> A hint of this emission is also possibly present in the B-mode observation of Rankin & Rathnasree (1995); however, we see nothing comparable in any of our much more sensitive B-mode sequences.

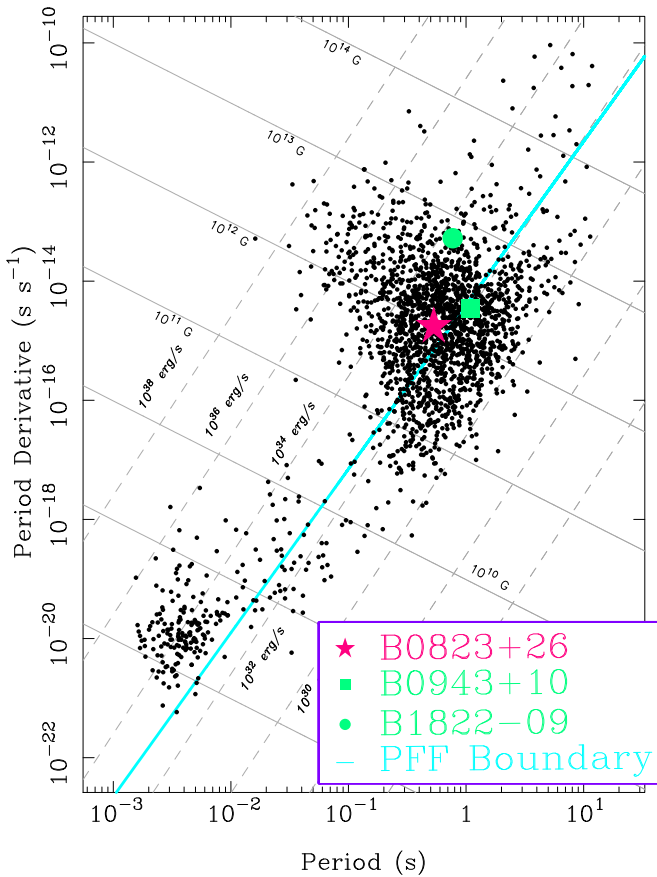


**Figure 14.**  $P$ - $\dot{P}$  diagram showing the transition between 2D and 3D polar cap configurations. Notice that pulsars B0823+26 and B0943+10 both fall near this transition line—whereas pulsar B1822-09 falls well to the left of it. The magnitudes of the surface magnetic field and spindown energy are also shown.

configurations, the former with a flat (2D) pair-formation front, and the latter with a 3D cup-shaped one. B0823+26 (denoted by the red star in Figure 14) nearly straddles the boundary and may barely have a flat PFF—or perhaps has something of a hybrid. In the bright mode, its PFF is primarily flat, centered, and energetic enough to generate the plasma associated both with core emission and backflow heating—and thus thermal X-rays—as well as some peripheral plasma producing much weaker conal emission. By contrast, in its quiet mode the 3D front produces the annular plasma supply needed for weak conal emission and tiny amounts of core-associated plasma or backflow heating. The “switch” between these two PFF configurations is mainly the gap potential, so is readily altered dynamically, perhaps assuming several stable magnetospheric equilibrium “states.”

The two different polar cap configurations appear to fundamentally underlie the distinction between core and conal emission. That the radio-frequency emission stems from turbulence produced by the two-stream instability of plasma “clouds” is largely accepted, and recent evidence points to its origin in highly nonlinear charged solitons (e.g., Lakoba et al. 2018; Mitra et al. 2016) radiating in dense plasma regions at frequencies lower than the plasma frequency. These emitting entities may well be produced under different conditions by the more energetic and axial flat PFF and the 3D cup-shaped configurations wherein field-line curvature and edge effects are maximized.

The two configurations seem beautifully drawn by the B0823+26 radio/X-ray results (Hermsen et al. 2018), where thermal X-rays were strongly emitted during the B mode and largely disappeared in Q-mode intervals. This scenario provides a further reason for the lack of IP X-ray flux in B0823+26: the IP profile appears to be entirely conal (though our sightline may miss any core beam), and thus its 3D PFF produces weak plasma and little backflow heating.

This scenario begins to account for the differences between B0823+26’s bright and weak modes in its MP region, but it gives little insight about how or why the B and Q modes start and stop.

These circumstances provide an opportunity to speculate about how the plasma-generation configurations of the polar cap give rise to the radio emission we observe from higher altitudes. Plasma generation above a flat PFF would seem to be centered along the magnetic axis, whereas in the 3D PFF it would be more peripheral. However, the heated polar cap “spot” seems to be significantly smaller than the size of the polar cap, so that the core-associated plasma may reflect a more specially confined current pattern. In any case, the conal emission is more peripheral, possibly subject to localized “spark” discharges and to  $\mathbf{E} \times \mathbf{B}$  drift.

## 7. Conclusions and Questions

Our study confirms aspects of earlier analyses by Rankin & Rathnasree (1995), Young et al. (2012), Sobey et al. (2015), and Basu & Mitra (2019) while extending these results in important ways. While it could hardly be doubted that B0823+26 is a near orthogonal rotator, we are able to strengthen this conclusion from several directions. Fortunately, B0823+26 shows a PPA traverse that can be tracked over much of its rotation cycle and well fitted by the RVM. This shows that its geometry is very closely an orthogonal rotator with  $\alpha$  close to  $90^\circ$  and  $\beta$  some  $3^\circ$  for the MP and perhaps  $5^\circ$  for the IP. Moreover, in this configuration the null surfaces interact with the polar flux tube at relatively low altitude, such that an “outer gap” accelerator may be active as a source of nonthermal X-rays in the B mode and perhaps radio-frequency emission in the Q.

Pulsar B0823+26 is a strong pulsar with extended intervals of bright and weak behavior that permit a considerable level of physical understanding. That the core-dominated bright mode is associated with a hot polar cap sustained by backflow heating cannot be doubted. However, this behavior seems supplemental to the conal-dominated quiet mode wherein the surface temperatures are too low to generate detectable X-rays.

Emission in the IP seems to be entirely conal, which probably explains why this second polar cap is cooler and thus not a significant source of thermal X-rays.

Quiet-mode emission would seem to be stable if uninterrupted by the B mode, but as Sobey et al. (2015) found, it too fails (nulls) for a time before B-mode onsets. How or why? What then prompts the B mode to start and fail? Once started it seems to persist for hours or days.

Finally, the possible changing circumstances between B0823+26’s bright and quiet modes may begin to explain our earlier results of radio/X-ray campaigns on pulsars B0943+10 (Hermsen et al. 2013; Mereghetti et al. 2016) and B1822-09 (Hermsen et al. 2017). As we have seen in Figure 14, pulsar B0823+26 falls very close to the 2D/3D pair-formation front boundary; however, so does the pulsar B0943+10. It is

possible that this pulsar’s radio “quiet”/X-ray bright (Q) mode is actually brighter in the radio than its “bright”/X-ray quiet (B) mode, but that we miss this strong radio emission because of the very peripheral sightline we have through its MP. In its highly organized B mode, we view its radiation on the conal periphery; however, if the “quiet” mode is mostly core radiation, our sightline would mostly miss its central beam. Interesting also is pulsar B1822–09, which Figure 14 shows is well into the flat PFF, core-dominated region; therefore, perhaps its changes in pulse modulation represent no change in the “flat” PFF configuration, and thus do not change the backflow heating and consequent X-ray flux. One other pulsar, B0329+54 (not shown—and too distant to be detectable in X-rays; Brinkman et al. 2019) also lies close to the boundary and exhibits mode changes in something of the manner of B0823+26, whereas pulsar B1944+17 (also not shown) lies far from the boundary in the 3D PFF region and emits no detectable X-rays.<sup>9</sup>

T.O. gratefully acknowledges support from the Vermont Space Grant Consortium Fellowship, and G.W. thanks the University of Manchester for granting visitor status. Portions of this work were carried out with support from US National Science Foundation Grant AST 18-14397. The National Astronomy and Ionosphere Center (aka Arecibo Observatory) is operated by the University of Central Florida under a cooperative agreement with the US National Science Foundation, and in alliance with Yang Enterprises and the Ana G. Méndez-Universidad Metropolitana. This work made use of the NASA ADS astronomical data system.

### Appendix Observations

The Arecibo Telescope in Puerto Rico with its Gregorian feed system and Mock spectrometer backends was used to make new observations of pulsar B0823+26, mainly at 327 MHz (*P* band) but also at 1.4 (*L* band) and 4.5 GHz (*C* band).

These observations were not conducted simultaneously with any X-ray observatory. Their purpose was rather to explore and clarify the nature of this pulsar’s radio modes, the modal transitions, and the subtle interactions between the various emission regions. Given that the Q mode is unusual and transitions more so, the program was optimized through use of Arecibo rise-to-set observations whenever possible.

These new observations use the instrument’s Gregorian feed system, 327 MHz (“*P* band”) or 1100–1700 MHz (“*L* band”) receivers, and Mock spectrometers. At 327 MHz, four Mock spectrometers sampling 12.5 MHz bands were used across the 50 MHz available bandpass. Four 86 MHz bands centered at 1170, 1420, 1520, and 1620 MHz were used at 1.4 GHz, and the lower three were usually free enough of RFI such that they could be added together to provide an approximate 250 MHz bandwidth nominally at 1400 MHz. The four Stokes parameters were formed off-line in software, corrected for interstellar dispersion and Faraday rotation, and various

<sup>9</sup> Nearby pulsar B1133+16 has also recently been detected in X-rays (Szary et al. 2017). Though it has a classic conal double profile, its  $B_{12}/P^2$  of 1.5 falls just below the boundary, and weak core emission has been identified in its single pulses (Young & Rankin 2012). In this case mode changing affecting the core-beam intensity would be difficult to detect given our peripheral sightline traverse.

**Table 3**  
B0823+26 Observations

MJD	Band	Length (pulses)	Mode	Notes
55522	<i>L</i>	1130	B	
57292	<i>C</i>	2257	B	
57900	<i>P</i>	17304	B	
57907	<i>P</i>	16672	B => Q	at pulse 15000
57914	<i>P</i>	13977	Q	
57915	<i>P</i>	14084	B	
58064	<i>L</i>	17371	Q	
58205	<i>P</i>	12189	Q	
58509	<i>P</i>	16743	B	Hi-res

instrumental polarization effects. Sufficient channels were used in each subband such that the instrumental resolutions of the observations are all about a milliperiod. However, for strong pulsars such as B0823+26 the Mock channel filters are not sharp enough to prevent aliasing, so we use only the central 2/3 of each channel. The PPAs are absolute in that they have been Faraday derotated to infinite frequency using rotation measures determined for each observation. However, at 327 MHz the errors prevent them from being precise, so small corrections were made to align them with the 1.4 GHz profiles. The band, MJDs, lengths, and modes of the observations are given in Table 3. Slow pulsars with small dispersion measures are more vulnerable to RFI than those of faster, more highly dispersed pulsars, so we have developed techniques to identify and remove the RFI from the pulse sequences, which are especially important for the weak Q mode.

### ORCID iDs

Joanna M. Rankin  <https://orcid.org/0000-0002-8923-6065>

### References

- Backer, D. C. 1973, *ApJL*, 182, 245  
 Basu, R., & Mitra, D. 2019, *MNRAS*, 487, 4536  
 Basu, R., Mitra, D., Melikidze, G. I., et al. 2016, *ApJL*, 833, 29  
 Basu, R., Mitra, D., & Rankin, J. M. 2015, *ApJL*, 798, 105  
 Becker, W., Weisskopf, M. C., Tennant, A. F., et al. 2004, *ApJL*, 615, 908  
 Blaskiewicz, M., Cordes, J. M., & Wassermann, I. 1991, *ApJL*, 370, 643  
 Brinkman, C., Dipanjan, M., & Rankin, J. 2019, *MNRAS*, 484, 2725  
 Craft, H. D., Lovelace, R. V. E., & Sutton, J. M. 1968, *IAU Circ.*, 2100, 1  
 Curtin, A., Weisberg, J. M., Rankin, J. M., & Venkataraman, A. 2020, *ApJ*, submitted  
 Deshpande, A. A., & Rankin, J. M., 2001, *MNRAS*, 322, 438  
 Dyks, J., Rudak, B., & Harding, A. K. 2004, *ApJL*, 607, 939  
 Everett, J. E., & Weisberg, J. M. 2001, *ApJL*, 553, 341  
 Gould, D. M., & Lyne, A. G. 1998, *MNRAS*, 301, 253  
 Hankins, T. H., & Fowler, L. A. 1986, *ApJL*, 304, 264  
 Hermsen, W., Kuiper, L., Basu, R., et al. 2018, *MNRAS*, 480, 3655  
 Hermsen, W., Kuiper, L., Hessels, J. W. T., et al. 2017, *MNRAS*, 466, 1688  
 Hermsen, W., Kuiper, L., van Leeuwen, J., et al. 2013, *Sci*, 339, 436  
 Komesaroff, M. M. 1970, *Natur*, 225, 612  
 Lakoba, T., Mitra, D., & Melikidze, G. 2018, *MNRAS*, 480, 4543  
 Lyne, A. G., Anderson, B., & Salter, M. J. 1982, *MNRAS*, 201, 503  
 Mereghetti, S., Kuiper, L., Tiengo, A., et al. 2016, *ApJL*, 831, 21  
 Mitra, D., Rankin, J., & Arjunwadkar, M. 2016, *MNRAS*, 460, 3063  
 Morris, D., Graham, D. A., Sieber, W., et al. 1979, *A&A*, 73, 46  
 Olszanski, T. E. E., Mitra, D., & Rankin, J. M. 2019, *MNRAS*, 489, 1543  
 Radhakrishnan, V., & Cooke, D. J. 1969, *ApL*, 3, 225  
 Radhakrishnan, V., & Rankin, J. M. 1990, *ApJL*, 352, 258  
 Rankin, J. M. 1993a, *ApJL*, 405, 285  
 Rankin, J. M. 1993b, *ApJS*, 85, 145  
 Rankin, J. M. 2007, *ApJL*, 664, 443  
 Rankin, J. M. 2015, *ApJL*, 804, 112

- Rankin, J. M., & Rathnasree, N. 1995, *JApA*, **16**, 327
- Sobey, C., Young, N. J., Hessels, W. T., et al. 2015, *MNRAS*, **451**, 2493
- Szary, A., Gil, J., Zhang, B., et al. 2017, *ApJL*, **835**, 178
- Timokhin, A. N., & Harding, A. K. 2015, *ApJL*, **810**, 144
- Weltevrede, P., & Johnston, S. 2008, *MNRAS*, **391**, 1210
- Weltevrede, P., Edwards, R. T., & Stappers, B. W. 2006, *A&A*, **445**, 243
- Weltevrede, P., Stappers, B. W., & Edwards, R. T. 2007, *A&A*, **469**, 607
- Young, N. J., Stappers, B. J., Weltevrede, P., Lyne, A. G., & Kramer, M. 2012, *MNRAS*, **427**, 114
- Young, S. A. E., & Rankin, J. M. 2012, *MNRAS*, **424**, 2477